The International Journal of Advanced Manufacturing Technology (2018) 96:3403–3416
https://doi.org/10.1007/s00170-018-1838-8

ORIGINAL ARTICLE

High-performance parallel hexapod-robotic light abrasive grinding using real-time tool deflection compensation and constant resultant force control

Masoud Latifinavid[1,2] · Abdulhamit Donder[1] · Erhan ilhan Konukseven[1]

Received: 6 November 2017 / Accepted: 25 February 2018 / Published online: 6 March 2018

Abstract
In robotic grinding, significant tool deflection occurs due to the lower stiffness of the manipulator and tool, compared with operation by universal grinding machines. Tool deflection during robotic grinding operation causes geometrical errors in the workpiece cross section. Also, it makes difficult to control the grinding cutting depth. In this study, a method is proposed for calculation of the tool deflection in normal and tangential directions based on grinding force feedback in these directions. Based on calculated values, a real-time tool deflection compensation (TDC) algorithm is developed and implemented. Force interaction between the tool and workpiece is significant for grinding operation. Implementing grinding with constant normal force is a well-known approach for improving surface quality. Tool deflection in the robotic grinding causes orientation between the force sensor reference frame and tool reference frame. This means that the measured normal and tangential forces by the sensor are not actual normal and tangential interaction forces between the tool and workpiece. In order to eliminate this problem, a resultant grinding force control strategy is designed and implemented for a parallel hexapod-robotic light abrasive surface grinding operation. Due to the nonlinear nature of the grinding operation, a supervised fuzzy controller is designed where the reference input is identified by the developed grinding force model. This grinding model is optimized for the robotic grinding operation considering setup stiffness. Evaluation of the experimental results demonstrates significant improvement in grinding operation accuracy using the proposed resultant force control strategy in parallel with a real-time TDC algorithm.

Keywords Robotic grinding · Resultant grinding force control · Supervised fuzzy control · Tool deflection compensation · Grinding force model

1 Introduction

Robotic machining systems have been researched for years to compromise between performance and flexibility for automated machining tasks such as grinding of jet engine turbine propellers. Despite providing great working capabilities on the complex paths of machining tasks, robotic machining setups have less stiffness compared with computer numerical control (CNC) machines. Tool deflection in robotic machining significantly affects the machining forces, machining accuracy, and surface quality. The machining setup stiffness and effects of setup, workpiece, and tool deflections in the operation performance as well as techniques of handling these effects have been researched [2, 3, 16–18]. In order to decrease dimensional errors due to the tool deflection in surface milling operations, a tool path selection method is developed in [10] based on minimization of tool deflection forces along the path. In this method, for three and five axis milling operations, the paths that result minimum tool deflection cutting force, which is defined in the plane of the tool axis and the normal vector to

✉ Erhan ilhan Konukseven
konuk@metu.edu.tr
Masoud Latifinavid
masoud.navid@metu.edu.tr
Abdulhamit Donder
adonder@metu.edu.tr

[1] Mechanical Engineering Department, Middle East Technical University, Dumlupinar Bulvari, No. 1, 06800 Cankaya/Ankara, Turkey

[2] Mechatronic Engineering Department, University of Turkish Aeronautical Association, Bahcekapi Quarter Okul Street, No.11, 06790 Etimesgut/Ankara, Turkey

the workpiece surface, are extracted. Implementing milling on these paths decreases dimensional errors. For three-axis milling, two options are proposed. The first is selecting a general path that minimizes the mean value of the tool deflection force and the second is selecting the various milling directions at each control node that results in less tool deflection force and connecting these nodes together. For the five-axis milling, both tool axis orientation and milling direction are considered in order to minimize the tool deflection force. In spite of higher accuracy-choosing proper tool path, the authors did not propose any algorithm for compensation of the tool deflection. In [35], a method is proposed for minimization of vibrations and cutting forces during ball end milling of hardened steel. This method is focused on optimal selection of tool overhang and surface inclination in order to minimize the cutting forces and vibrations and improve the surface quality of machined workpiece. The results of this research show that increasing the tool overhang causes an increase of acceleration of vibration amplitudes. Also, the results of this research indicate that increasing the surface inclination causes to decrease of cutting forces where the maximum value for cutting forces is obtained during slot milling with zero inclination. The surface inclination effect together with cutting speed effect is investigated in [34] during ball end milling of hardened steel. Optimum values are proposed for cutting speed and surface inclination for minimization of cutting forces. Such a minimization in cutting forces decreases the tool deflection and improves the machining accuracy. The focus of both mentioned researches is on optimization of machining parameters with respect to the workpiece surface profile, but compensation of the tool deflection is not considered. In ultra-precision machining, the effect of workpiece material properties is more important in comparison with that of conventional machining because the depth of cut changes in sub-micrometer range [6]. The effect of elastic recovery of workpiece material on surface roughness during ultra-precision milling is investigated in [33]. The results of this research revealed that the elastic recovery capability of workpiece material improves the surface finish in ultra-precision raster milling. The static stiffness of different points of workpiece is calculated, and the surface topography of these points after precise turning is investigated in [21]. The results reveal the considerable effect of stiffness on surface roughness. In most of the experiments, the surface quality is better at the points with higher stiffness and less deflection.

There are several studies in the literature related to the compensation of tool deflection effects on workpiece. In this section, a review of the different strategies of these studies is presented. Most of the mentioned studies are related to end-milling operation. Kline et al. [9] proposed a method for predicting the amount of tool and workpiece deflection in end-milling operation based on cantilever beam theory. A force model and cantilever beam theory were used to obtain the amount of deflection. Similarly, Ryu et al. [28] investigated side will machining operation and attempted to predict the errors caused by tool deflection. However, a solution for compensation of these errors was not presented. The effect of the workpiece curvature on tool deflection and the resulting surface errors were investigated in [26]. A method based on path correction was proposed by Law et al. [12]. Their aim was to decrease tool deflection and its effect on the workpiece using an optimum tool path. Approaches for path correction in end-milling operations were presented in [4, 29, 30] and [7] by adding an offset to the tool path. Cantilever beam theory was used to calculate the amount of tool deflection. Rao et al. [27] proposed an iterative approach instead of a single offset to compensate for offset error caused by tool deflection. However, tool angle compensation was not investigated. A method for compensation of tool angle and tool displacement during end-milling operation was proposed by Yang et al. [36] where a proximity sensor was used for detecting tool deflection. A strong aspect of their research is that they considered both tool angle and tool tip displacement by compensating errors.

1.1 Constant force control

In recent years, force control during robotic machining has been significant for the proper execution of the operation tasks [1, 38]. In these tasks, the robot is controlled to maintain a given set force while the deflection of the robotic arm and cutting tool are major factors that should be considered. In [15], a force control system was designed to reduce the surface roughness by decreasing grinding force variation. A PID controller was used without considering tool and setup deflections during the process where the force sensor is mounted under the workpiece. A constant normal force control technique was developed by the authors. A normal force control on robotic grinding and deburring was investigated by Domroes et al. in [5]. They tried to maintain a constant normal force by adjusting the feed rate. However, they did not offer a systematic procedure for defining the reference force. Also, the stiffness of the setup and workpiece was not investigated. In [25], an adaptive control strategy for surface finishing was studied in which the goal was to track the desired motion in the tangential direction and regulate the desired force normal to the surface simultaneously. For this purpose, a dynamic model of the robot was generated. Using the dynamic model, a control scheme was developed that adapts the grinding coefficient, which is the relationship between the normal and tangential forces. The designed controller was tested on straight and curved surfaces. Thomessen

et al. proposed a strategy to control the normal grinding force by simultaneously adjusting the position and feed rate of the tool [32]. Active control force feedback was used in grinding of large Francis turbines where the force sensor was located behind the end effector of the manipulator. However, a user-defined reference force was used during experiments. Despite the large normal grinding force values, the effects of tool deflection and resulting errors on the sensor reference frame were not considered. An automatic grinding system using a hand grinder and a CNC machine was investigated by Liu et al. in [14]. Compliance of the grinding system was considered by modelling the stiffness of each component using a mass spring model. The real-time normal force feedback was supplied by a force sensor located under the workpiece. For normal grinding force control, a PID controller was used. A linear relationship between the cut depth and the normal force was assumed, and the slope of the cut depth-normal force graph was used as a stiffness of material removal process.

There are two options for the placement of force sensors for grinding operation. The first option is mounting the sensor under the workpiece. The advantage of this option is that there is no orientation between the sensor reference frame and workpiece reference frame. This means that the measured normal and tangential grinding forces by the sensor are real normal and tangential interaction forces between the tool and workpiece. However, in grinding of larger workpieces, it is not functional to use a sensor under the workpiece. The second option is placing the force sensor behind the spindle. This option is useful for industrial grinding applications using robot manipulators. But, in robotic grinding, due to deflection of the tool, there is an orientation between the sensor reference frame and tool reference frame. This means that the measured values for normal and tangential forces are not the real normal and tangential interaction forces between the tool and workpiece. In this study, the second option is selected for mounting the force sensor. In order to solve the problem caused by the tool reference frame orientation, the resultant grinding force was selected as a control parameter.

There is limited research on the effects of resultant force control in machining. An adaptive controller was developed by Budak to control the resultant force of milling operations [1]. A significant improvement was observed in the surface quality of the workpiece using the resultant force control algorithm. An adaptive control strategy was used in [8] to maintain a constant resultant force while implementing robotic deburring. The proposed approach showed promising results in force/position tracking of an unknown environment. Although normal force control in robotic grinding is a research field that is often investigated, model-supervised resultant force control is not studied in detail. In this study, model-supervised resultant force control is studied in order to improve surface quality.

1.2 Control approaches

Designed linear controllers, such as PID, can be tuned and used in certain grinding conditions. However, due to the non-linearity of the grinding process, the mentioned linear controllers do not turn out a comprehensive solution. Fuzzy controller or a combination of fuzzy and PID controllers are preferable solutions for force control during grinding operations. A hybrid force motion control architecture is proposed in [20] for increasing robot autonomy. The performances of PI and fuzzy PI controllers were compared, and fuzzy PI controller showed better efficiency. A fuzzy controller is used for force control of a ceramic grinding (Al2O3) process in [19]. The results showed a more stable machining process when fuzzy controllers were used. Li et al. proposed an adaptive fuzzy control algorithm for hard sphere grinding [13]. Instead of a force sensor, a model was used to estimate the grinding force based on the spindle current indirectly. Based on the grinding force, the cut depth and spindle speed were controlled with a dynamic threshold-based fuzzy adaptive control approach. Although spindle current is used as a key factor for estimation of the grinding force, the obtained model cannot be used for different setups and spindles. This is because of the different characteristics of different spindles. The same current value can correspond to different grinding force bands when the spindle types are different. In our study, a factor called percent load is used in the grinding force model instead of spindle current. A fuzzy PID controller for grinding and deburring applications was generated in [31, 37]. The parameters of the PID controller were updated online at each sampling time by fuzzy rules.

In this study, a combination of a robotic grinding force model and a fuzzy control strategy is developed to maintain a constant resultant grinding force during robotic grinding operation. The grinding model used is optimized for robotic grinding applications considering the setup and tool and workpiece stiffness. As a result, a realistic reference force is generated for the fuzzy controller. Also, an approach is utilized for calculating tool deflection values as a function of grinding forces in the normal and tangential directions. A kinematic solution is proposed for real-time tool deflection compensation (TDC).

2 Effect of tool deflection on robotic surface grinding forces

Grinding with constant normal force and constant tangential velocity is a well-known approach for increasing operation

accuracy and obtaining constant cutting depth and surface quality along the workpiece. However, the mentioned approach is effective when using universal grinding machines that are very stiff and the deflection of the tool and setup is negligible. In the case of robotic grinding, the stiffness of the robot and setup is lower than that of CNC-type grinding machines. Consequently, there are considerable tool and setup deflections that have significant effects on the grinding forces. During grinding with CNC - type machines, when there is a flat workpiece profile and the grinding parameters (depth of cut, spindle speed, and feed rate) are constant, the grinding normal and tangential forces are expected to be constant. However, in robotic grinding, due to lower stiffness and tool-setup deflection, the grinding forces can show three different characteristics through the workpiece profile even when the grinding parameters are constant and the workpiece has a flat surface profile [11]. The three characteristics are classified in three regimes in Ref. [11]. These regimes are identified based on variation of a grinding force pattern during the surface grinding experiments. By the grinding parameters (feed rate, spindle speed, and depth of cut) or by changing the stiffness of the grinding robot, tool, and workpiece, one of the regimes can occur. In the first regime, the grinding forces remain almost constant because the tool is able to cut the workpiece at a constant feed rate (Fig. 1a). The factors that lead to obtain constant grinding forces (regime 1 in surface grinding) are low feed rate, low depth of cut, high spindle speed, and high stiffness of grinding machine. During the surface grinding operation, the forces increase almost linearly in the second grinding regime (Fig. 1b). If significant tool deflection occurs, this grinding regime is observed. The factors that lead to obtain ascending grinding forces (regime 2 in surface grinding) are high feed rate, high depth of cut, low spindle speed, and low stiffness of grinding machine. The third grinding is a transition between the first and second regimes. In this regime, force fluctuations occur during the operation (Fig. 1c). The force fluctuations take place because of small tool deflections followed by fast deflection compensation that frequently occur during grinding experiments.

The differences between the characteristics of robotic grinding and CNC grinding show the effects of tool deflection and setup stiffness on normal and tangential force behaviors. In grinding operations with force feedback, the force sensor is commonly mounted behind the spindle or behind the workpiece. If tool deflection occurs, an orientation occurs between the tool tip reference frame and the force sensor reference frame, as shown in Fig. 2. This tool deflection can be expressed as two orientations around the Y_{sensor} axis (β_t) and Z_{sensor} axis (γ_t). In this case, the measured normal and tangential grinding forces are not the grinding forces of the tool reference frame because of the orientation. Force changes caused by the deflection cause an undesired variation of cutting depth along the workpiece. The other important effect of tool deflection is geometrical errors in the cross section of the workpiece. The contact angle between the tool and workpiece changes the cutting depth in the cross section of the workpiece.

3 Experimental setup

In this research, an experimental setup was designed. The setup consisted of a PI H-824 hexapod, PI P-602 piezo move flexure actuator, ATI Gamma IP60 Force/ Torque sensor, high-frequency BMR 222-42-MHM spindle, CBN ZY 4.0-5 B126 tool (tool diameter 4 mm, overhang 25 mm), workpiece (St37 steel), tool changer, and collets (Fig. 3). The 6-DOF parallel robot that is used in this study has $7N/\mu m$ stiffness in tangential direction (y direction) and $1.7N/\mu m$ stiffness in the normal direction (z direction). The repeatability of the hexapod in normal and tangential directions is $0.1\mu m$ and $\pm 0.5\mu m$ and the single actuator design resolution of the hexapod is $0.007\mu m$. The resolution of the force/torque sensor in tangential and normal directions is 0.00625 and $0.0125N$. Stiffness of the

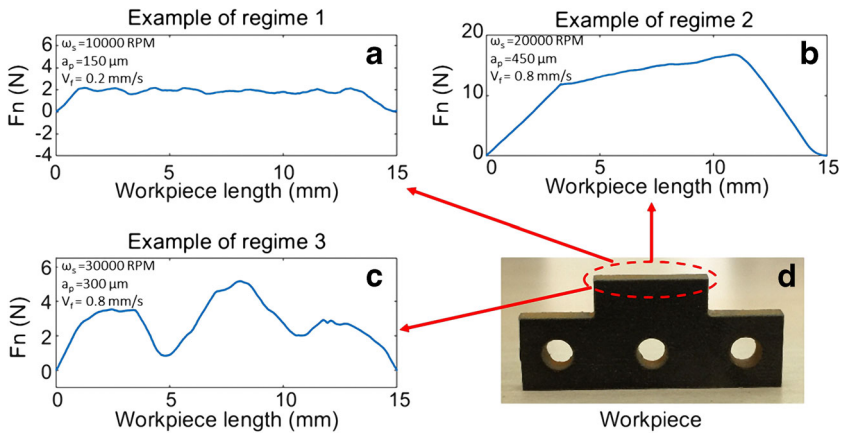

Fig. 1 Regime 1 example (**a**), regime 2 example (**b**), regime 3 example (**c**), workpiece (**d**)

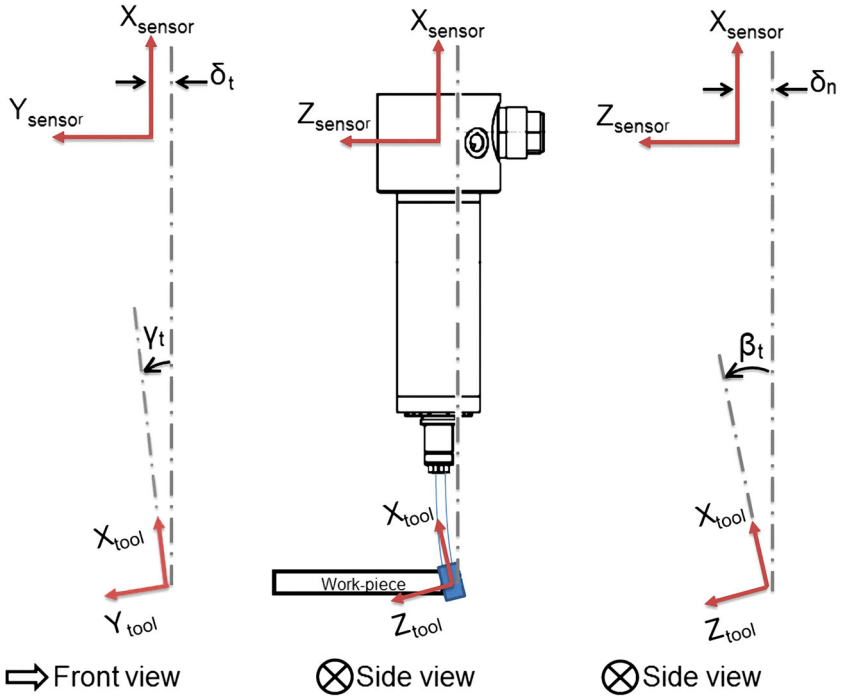

Fig. 2 Orientations between the tool tip reference frame and force sensor reference frame

force/torque sensor in normal and tangential directions is 18 and $9.1 N/\mu m$. Head stiffness of the spindle is negligible. The force/torque sensor and parallel hexapod are notably stiff, and they are accurate enough to cover the range of parameters for the grinding experiments conducted in this study. The maximum nominal output power of the used electro-spindle is $300 W$ and the maximum rotational speed is 60000 rpm. In addition to the 6-DoF parallel manipulator, the experimental setup has an additional 1 degree of freedom that is actuated by a piezo actuator. The actuator is fixed to the properly constrained table, presenting a single degree of freedom in the z-direction as shown in Fig. 3. While performing grinding in the y-direction as shown in Fig. 3, the machining errors can be reduced by admittance control-based negative compensation by the actuation of the piezo actuator.

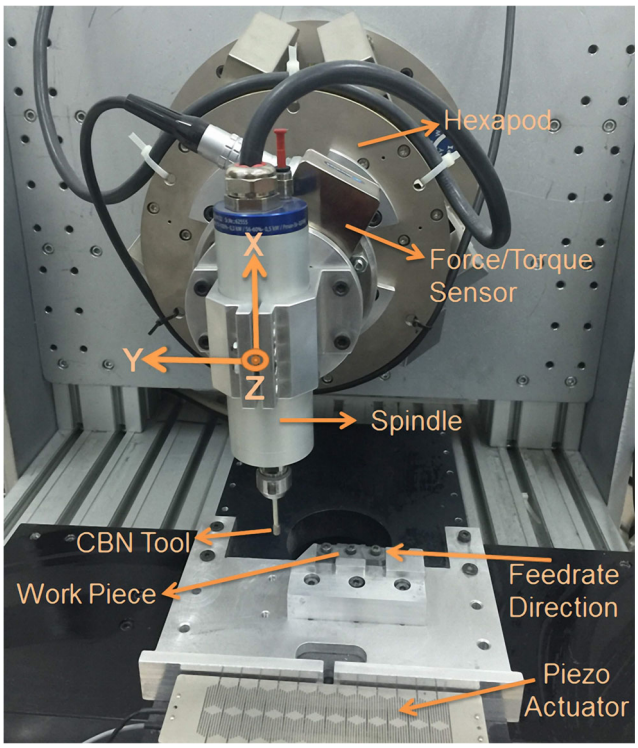

Fig. 3 Experimental setup

4 Modelling tool deflection

In this section, the model developed for tool orientation and displacement in the normal and tangential directions is explained. The tool-workpiece interaction and their reaction parameters are shown in Fig. 4. Assuming that the spindle

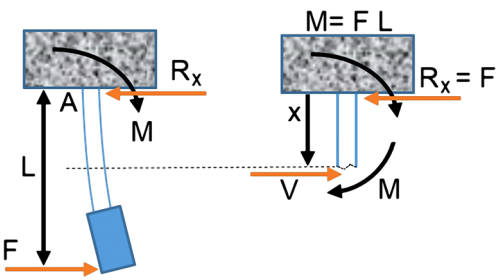

Fig. 4 Tool modeled as a cantilever rod (left). Internal moment at x distance from the tool holder is shown (right)

and the robot are rigid and that the tool has a finite rigidity, the tool can be modelled as a cantilever rod where the internal moment at a distance of x from the tool holder (point A) can be represented as M.

To calculate the deflection and stiffness, the double integration method is utilized:

$$EI\frac{d^2\delta}{dx^2} = -M \tag{1}$$

where

E modulus of elasticity
I Moment of inertia
δ displacement
x distance from point A

The following equilibrium equation can be written:

$$-Fx + FL + M = 0 \tag{2}$$

so,

$$M = Fx - FL \tag{3}$$

Substituting Eq. 3 into Eq. 1 and implementing the double integration method, Eqs. 4–6 can be written.

$$EI\frac{d^2\delta}{dx^2} = FL - Fx \tag{4}$$

$$EI\frac{d\delta}{dx} = F\ L\ x - \frac{Fx^2}{2} + C_1 \tag{5}$$

$$EI\delta = \frac{F\ L\ x^2}{2} - \frac{F\ x^3}{6} + C_1x + C_2 \tag{6}$$

where C_1 and C_2 are constants. Implementing boundary conditions:

$$\text{For} \quad x = 0 \quad \begin{cases} \delta = 0 \rightarrow C_2 = 0 \\ \frac{d\delta}{dx} = 0 \rightarrow C_1 = 0 \end{cases} \tag{7}$$

As a result:

$$\frac{d\delta}{dx} = \frac{F}{EI}\left(Lx - \frac{x^2}{2}\right) \tag{8}$$

$$\delta = \frac{F}{2EI}\left(Lx^2 - \frac{x^3}{3}\right) \tag{9}$$

Maximum deflection and slope occur at the end of the tool where $x = L$.

In normal direction, considering $F = F_n$, tool tip displacement (δ_n) and tool deflection (β_t) are obtained as Eqs. 10 and 11.

$$\delta_n = \frac{F_nL^3}{3EI} \tag{10}$$

$$\beta_t = \frac{F_nL^2}{2EI} \tag{11}$$

In tangential direction, considering $F = F_t$, tool tip displacement (δ_t) and tool deflection (γ_t) are obtained as Eqs. 12 and 13.

$$\delta_t = \frac{F_tL^3}{3EI} \tag{12}$$

$$\gamma_t = \frac{F_tL^2}{2EI} \tag{13}$$

5 Kinematic solution for tool deflection compensation

In order to develop a kinematic solution for TDC, the exact position and orientation of the tool tip should be identified with respect to the hexapod reference frame. Then, it is possible to determine the new position and orientation for the hexapod aiming to compensate for geometrical errors caused by tool deflection. For this purpose, five reference frames are defined in the setup. The first reference frame (R_{base}) is the base reference frame, which is defined at the center of the hexapod top plate when it is in home position without any rotation or translation. R_{base} is fixed at this point and acts as the global coordinate system. The second frame (R_{hex}) is defined at the center of the top plate of the hexapod and moves with it. The third frame (R_{spn}) is defined as the tool holder of the spindle. The fourth and fifth reference frames (R_{tan} and R_{nor}) are assigned to the tool tip. The last two reference frames are related to the tool deflection in normal and tangental directions with respect to the R_{spn}. The side and front views of the setup and assigned reference frames are shown in Fig. 5.

The reference frames from the base frame to the tool tip are shown in Eq. 14.

$$R_{\text{base}} \rightarrow R_{\text{hex}} \rightarrow R_{\text{spn}} \rightarrow R_{tan} \rightarrow R_{nor} \tag{14}$$

Let $C^{(i,j)}$ be the rotation matrix of the j^{th} reference frame with respect to the i^{th} reference frame.

In this paper, the rotation matrices are written as exponential rotation matrix in the general form of $e^{\tilde{u}\theta}$ as in [22, 23]. It expresses a rotation of an angle θ about axis n, which is a unit column matrix. Here, $\tilde{u}$ represents a skew symmetric matrix corresponding to the unit vector n.

$$u = \begin{bmatrix} u_1 \\ u_2 \\ u_3 \end{bmatrix} \rightarrow \tilde{u} = \begin{bmatrix} 0 & -u_3 & u_2 \\ u_3 & 0 & -u_1 \\ -u_2 & u_1 & 0 \end{bmatrix} \tag{15}$$

The expansion of the exponential rotation matrix about axis n with angle θ is known as the Rodrigues formula, as in Eq. 16.

$$e^{\tilde{u}\theta} = I\ cos\ \theta + \tilde{u}\ sin\ \theta + uu^T\ (1 - cos\ \theta) \tag{16}$$

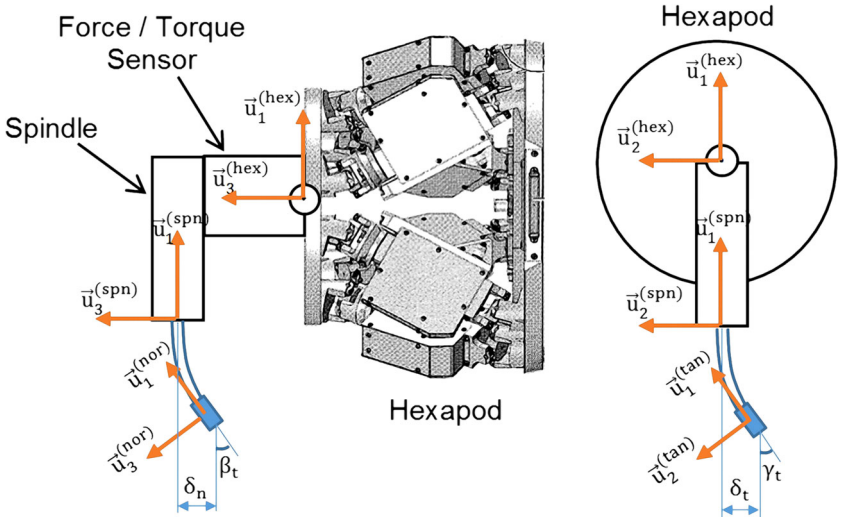

Fig. 5 Illustration of the setup and assigned reference frames

Also, u_i is defined as the i^{th} basic column matrix, which is the column matrix representation of the i^{th} unit basis vector $\overrightarrow{u}_i^{(k)}$ in reference frame R_k that is its own reference frame [24].

$$u_i = u_i^{(k/k)} = \left\{ \overrightarrow{u}_i^{(k)} \right\} |_{R_k} \tag{17}$$

Considering the end axis of the assigned reference frames indicated in Fig. 5 and the expression of the rotation matrices. The rotation matrix from R_{hex} to R_{nor} can be expressed as follows:

$$\hat{C}^{(hex,nor)} = \hat{C}^{(hex,spn)} \hat{C}^{(spn,tan)} \hat{C}^{(tan,nor)} \tag{18}$$

Considering assembly errors, the position and orientation of the spindle tool holder with respect to the hexapod reference frame are identified using a coordinate measurement machine (CMM). Consequently, the rotation matrix from R_{hex} to R_{spn} can be written as Eq. 19.

$$\hat{C}^{(hex,spn)} = \hat{C}_{CMM} \tag{19}$$

where $\hat{C}_{CMM}$ is a constant rotation matrix that expresses the orientation of the spindle with respect to the hexapod moving plate.

Tool deflection can be decoupled to two successive rotations in the tangential and normal directions. Note that both of the mentioned rotations occur about unit vectors of the spindle reference frame. γ_t is the rotation of the tool around the z-axis (u_3) of R_{spn} due to deflection in the tangential direction. So the rotation matrix from R_{spn} to R_{tan} can be written as Eq. 20.

$$\hat{C}^{(spn,tan)} = e^{\left(\tilde{u}_3^{(spn/spn)} \ \gamma_t\right)} \tag{20}$$

β_t is rotation about the y-axis (u_2) of R_{spn} due to deflection in the normal direction. So, the rotation matrix from R_{tan} to R_{nor} can be written as Eq. 21.

$$\hat{C}^{(tan,nor)} = e^{\left(\tilde{u}_2^{(spn/tan)} \ \beta_t\right)} \tag{21}$$

Equation 21 should be expressed in the spindle reference frame as follows:

$$e^{\left(\tilde{u}_2^{(spn/tan)} \ \beta_t\right)} = \hat{C}^{(tan,spn)} e^{\left(\tilde{u}_2^{(spn/tan)} \ \beta_t\right)} \hat{C}^{(spn,tan)} \tag{22}$$

Considering Eq. 23 as:

$$\hat{C}^{(tan,spn)} = e^{-\left(\tilde{u}_3^{(spn/spn)} \ \gamma_t\right)} \tag{23}$$

so, Eq. 22 will change to Eq. 24.

$$e^{\left(\tilde{u}_2^{(spn/tan)} \ \beta_t\right)} = e^{-\left(\tilde{u}_3^{(spn/spn)} \ \gamma_t\right)} e^{\left(\tilde{u}_2^{(spn/spn)} \ \beta_t\right)} e^{\left(\tilde{u}_3^{(spn/spn)} \ \gamma_t\right)} \tag{24}$$

Tool deflections in both the tangential and normal directions are expressed in the spindle reference frame. Consequently, substituting Eqs. 19, 20, and 24 into the Eq. 18, rotation matrix from hexapod to tool tip ($\hat{C}^{(hex,nor)}$) can be obtained as follows: Simplifying $\tilde{u}_i^{(spn/spn)}$ as $\tilde{u}_i$, consequently:

$$\hat{C}^{(hex,nor)} = \hat{C}_{CMM} \, e^{(\tilde{u}_3 \ \gamma_t)} e^{-(\tilde{u}_3 \ \gamma_t)} e^{(\tilde{u}_2 \ \beta_t)} e^{(\tilde{u}_3 \ \gamma_t)} \tag{25}$$

given

$$e^{(\tilde{u}_3 \ \gamma_t)} e^{-(\tilde{u}_3 \ \gamma_t)} = \hat{I} \tag{26}$$

$$\hat{C}^{(hex,nor)} = \hat{C}_{CMM} \, e^{(\tilde{u}_2 \ \beta_t)} e^{(\tilde{u}_3 \ \gamma_t)} \tag{27}$$

Let t_{spn}^{hex} be the translation from the hexapod reference frame to the spindle reference frame obtained by CMM.

$$t_{spn}^{hex} = \begin{bmatrix} r_x \\ r_y \\ r_z \end{bmatrix} \tag{28}$$

Considering the assigned reference frames and tool deflection, the translation from the hexapod reference frame to the tool tip can be written as Eq. 29. Based on the feeding direction, δ_t can be a positive or negative value. Here, δ_n is

always a negative value because the normal grinding force and z-axis are in opposite directions.

$$t_{nor}^{spn} = \begin{bmatrix} -L\cos\gamma_t\cos\beta_t \\ \delta_t \\ \delta_n \end{bmatrix} \tag{29}$$

Consequently, the translation matrix and transformation homogenous matrix from R_{hex} to R_{nor} are as follows:

$$t_{nor}^{hex} = \begin{bmatrix} r_x - L\cos\gamma_t\cos\beta_t \\ r_y + \delta_t \\ r_z + \delta_n \end{bmatrix} \tag{30}$$

$$T_{nor}^{hex} = \begin{bmatrix} \hat{C}^{(hex,nor)} & t_{nor}^{hex} \\ 0\ 0\ 0 & 1 \end{bmatrix} \tag{31}$$

In order to obtain the forward kinematics of the robotic grinding setup, the transformation homogenous matrix should be written in the base reference frame. This means the rotation and translation of the hexapod moving plate with respect to the base frame should be considered. Considering the transformation homogenous matrix from R_{base} to R_{hex} as T_{hex}^{base}:

$$T_{hex}^{base} = \begin{bmatrix} \hat{C}_{hex} & t_{hex}^{base} \\ 0\ 0\ 0 & 1 \end{bmatrix} \tag{32}$$

where $\hat{C}_{hex}$ and t_{hex}^{base} are the orientation and translation matrices of the hexapod moving plate and can be controlled in real-time. The forward kinematics of the robotic grinding setup can be defined as T_{FK} and obtained by multiplication of T_{hex}^{base} to T_{nor}^{hex}.

$$T_{FK} = T_{hex}^{base}\ T_{nor}^{hex} \tag{33}$$

The transformation homogenous matrix for hexapod that maintains the desired position and orientation of the tool tip can be defined as ($T_{new-hex}^{base}$). The desired forward kinematics of the setup is $T_{FK-desired}$. Therefore,

$$T_{new-hex}^{base}\ \ T_{nor}^{hex} = T_{FK-desired} \tag{34}$$

Finally, multiplying the desired forward kinematics with the inverse of T_{nor}^{hex}, a new position and orientation of the hexapod are obtained that compensate for the geometrical errors due to tool deflection.

$$T_{new-hex}^{base} = T_{FK-desired}\ \ T_{nor}^{hex^{-1}} \tag{35}$$

In this study, the desired orientation for the tool is to maintain the vertical direction. Therefore, all of the calculations during operation are made with this goal. In our setup, the calculated new rotation matrix for the hexapod should be changed to the Euler angles 1-2-3 sequence format to use as the input to the robot. In the next section, the resultant force control strategy is explained, which is implemented in parallel with the TDC approach.

6 Constant resultant force control using model-supervised fuzzy controller

In the previous section, the effect of tool deflection is investigated and a kinematic solution is proposed. The

Table 1 Descriptions of model parameters

Symbol	Description
a_p	Depth of cut
d_e	Tool diameter
A_{1ft}	Area under F_t graph from start time to peak time
A_{1fn}	Area under F_n graph from start time to peak time
A_{2ft}	Area under F_t graph from peak time to end time
A_{2fn}	Area under F_n graph from peak time to end time
ΔA_{ft}	$A_{1ft} - A_{2ft}$
ΔA_{fn}	$A_{1fn} - A_{2fn}$
F_t	Tangential grinding force
F_n	Normal grinding force
F_{pt}	Peak F_t value
F_{pn}	Peak F_n value
I_s	Spindle current
L_p	Percent load of the spindle. If the spindle is not loaded and no defect exists, the L_p will equal to 0%
$L_{p_{max}}$	Peak L_p value of penetration test
t_{1ft}	Difference between peak time and start time of t-F_t graph (ascending period)
t_{2ft}	Difference between end time and peak time of t-F_t graph (descending period)
t_{1fn}	Difference between peak time and start time of t-F_n graph (ascending period)
t_{2fn}	Difference between end time and peak time of t-F_n graph (descending period)
t_{pft}	Peak time of F_t graph
t_{pfn}	Peak time of F_n graph
V_f	Feed rate
V_s	Velocity of tool wheel periphery (m/s)
ω_s	Spindle speed (RPM)

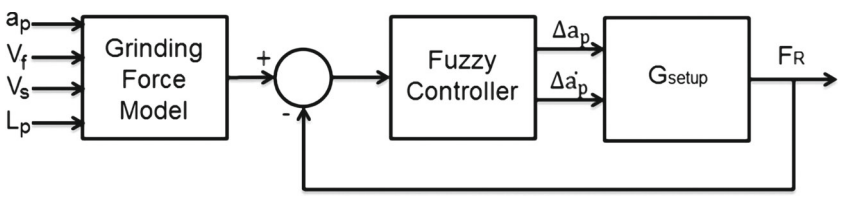

Fig. 6 Architecture of the proposed model-supervised fuzzy admittance controller

normal and tangential grinding forces measured by the sensor were shown not to be the grinding forces of the tool reference frame because of the mentioned orientations related to the tool deflection. Therefore, controlling the force in the normal direction of the force sensor reference frame is not a proper approach. This is the reason that the resultant of the grinding force components (normal and tangential forces measured by the sensor) is controlled instead of the normal force.

The robotic grinding operation has a highly nonlinear nature as shown in the previous section. Therefore, designing a control architecture that needs to be able to maintain a constant resultant grinding force is challenging. The conventional linear fixed-gain PID controllers can be optimized easily for desired control specifications such as overshoot, rise time, and settling time. Due to the nonlinearity of the grinding process, application of a PID controller with constant gains is not a proper approach and the gains should be modified continuously while handling different inputs and operating conditions. Even if the PID controller is optimized and used for certain conditions, implementation of the controller on a physical setup is challenging. In the physical setup, there are three input sources that should be considered. The first source is the parallel hexapod by which the grinding path and feed rate are controlled. The second source is the piezo actuator by which the depth of cut is controlled. The third source is the force sensor that supplies the force feedback. All of them have different response times. The controller should be able to synchronize the model and physical setup and control the setup force response in such a way that it converges to the model output that acts as the reference input.

In this study, a model supervised fuzzy control architecture was designed. For the user-defined set depth of cut (SDOC), spindle speed, feed rate, and average spindle percent load, the model gives the proper reference resultant grinding force. The aim of the model-supervised controller is to make the physical setup interaction resultant force converge with the reference value provided by the model. The depth of cut and its rate of change are the controlled parameters that are output by the fuzzy controller. During the operation together with the resultant force controller, the TDC algorithm is also used.

6.1 Grinding force model

The resultant force in grinding operation is the sum squared root of the normal and tangential forces, which is to be controlled. In order to design and optimize a controller, a grinding force model is defined. In robotic grinding, due to the effect of tool deflection and setup stiffness, the grinding model should be able to predict the forces in the different regimes mentioned in Section 2. In [11], an optimized force model for robotic grinding is proposed. In this model, using penetration tests and extracting the defined features, the mechanical properties of the setup and workpiece are included in the model indirectly. Also in this model, the percent load of the spindle, which is a function of spindle current, is included as an extra predictor in the model. The mentioned model is used in this study as a reference

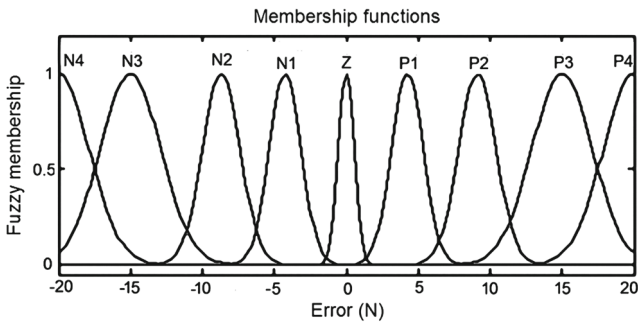

Fig. 7 Membership functions of Error

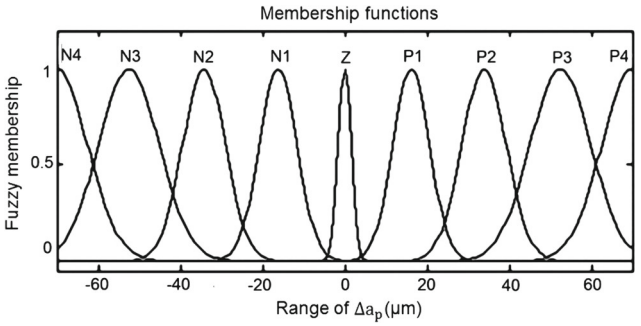

Fig. 8 Membership functions of (Δa_p)

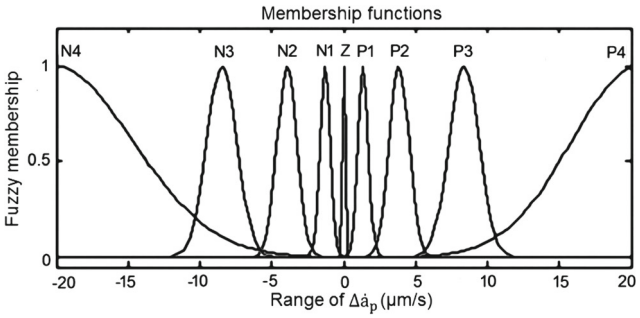

Fig. 9 Membership functions of $(\Delta \dot{a}_p)$

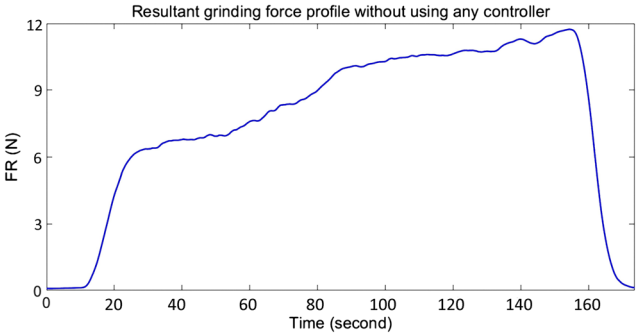

Fig. 10 Grinding resultant force profile without using a force controller

(required force components) input generator. The equations of normal and tangential grinding forces are as follows:

$$F_t = -4.67 - 37.1\left(\frac{b\,a_p\,V_f}{V_s}\right) + 0.505\left(\frac{b\,a_p\,V_f}{V_s}\right) ln\left(\frac{{V_s}^{1.5}}{{a_p}^{0.25}\,{V_f}^{0.5}}\right) + 0.0228\left(b\sqrt{d_e\,a_p}\right) + 1631\left(\frac{b\,V_f\sqrt{d_e\,a_p}}{V_s\,d_e}\right) + 0.465\left(\frac{A_{1ft}}{t_{1ft}}\right) - 1.15\left(\frac{A_{2ft}}{t_{2ft}}\right) + 0.311\left(L_p\,\frac{F_{pt}}{L_{p_{max}}}\right) \quad (36)$$

$$F_n = -4.42 - 155\left(\frac{b\,a_p\,V_f}{V_s}\right) + 10.5\left(\frac{b\,a_p\,V_f}{V_s}\right) ln\left(\frac{{V_s}^{1.5}}{{a_p}^{0.25}\,{V_f}^{0.5}}\right) + 2317\left(\frac{b\,V_f}{V_s}\sqrt{\frac{a_p}{d_e}}\right) + 1.49\left(\frac{A_{1fn}}{t_{1fn}}\right) - 4.24\left(\frac{A_{2fn}}{t_{2fn}}\right) + 1.79\left(L_p\,\frac{F_{pn}}{L_{p_{max}}}\right) \quad (37)$$

Table 2 Rule bases of the fuzzy controller

No	Rule bases
1	If $(Error\ is\ N4)$ then $(\Delta a_p\ is\ N4)$ and $(\Delta \dot{a}_p)\ is\ N4$
2	If $(Error\ is\ N3)$ then $(\Delta a_p\ is\ N3)$ and $(\Delta \dot{a}_p)\ is\ N3$
3	If $(Error\ is\ N2)$ then $(\Delta a_p\ is\ N2)$ and $(\Delta \dot{a}_p)\ is\ N2$
4	If $(Error\ is\ N1)$ then $(\Delta a_p\ is\ N1)$ and $(\Delta \dot{a}_p)\ is\ N1$
5	If $(Error\ is\ Z)$ then $(\Delta a_p\ is\ Z)$ and $(\Delta \dot{a}_p)\ is\ Z$
6	If $(Error\ is\ P1)$ then $(\Delta a_p\ is\ P1)$ and $(\Delta \dot{a}_p)\ is\ P1$
7	If $(Error\ is\ P2)$ then $(\Delta a_p\ is\ P2)$ and $(\Delta \dot{a}_p)\ is\ P2$
8	If $(Error\ is\ P3)$ then $(\Delta a_p\ is\ P3)$ and $(\Delta \dot{a}_p)\ is\ P3$
9	If $(Error\ is\ P4)$ then $(\Delta a_p\ is\ P4)$ and $(\Delta \dot{a}_p)\ is\ P4$

The descriptions of the model parameters are mentioned in Table 1. The parameter L_p represents the percent load of the spindle.

$$L_p = \frac{I_s - I_{s_0}}{I_{s_{100}} - I_{s_0}} \times 100 \quad (38)$$

In the percent load equation, I_{s_0} is the spindle current without any load and I_{s_100} is the spindle current for full load. These are spindle characteristics and can be derived from the spindle datasheet or by experiment for each speed base [11].

The details of the grinding force model are explained in [11].

6.2 Fuzzy controller design

In order to obtain desired cutting depth (SDOC) a resultant grinding force control strategy is used. The reference value for resultant grinding force is generated by the grinding force model where the inputs of the force model are desired depth of cut (SDOC), spindle speed, feed rate, and average spindle percent load. The output of the model is proper reference resultant grinding force. The physical

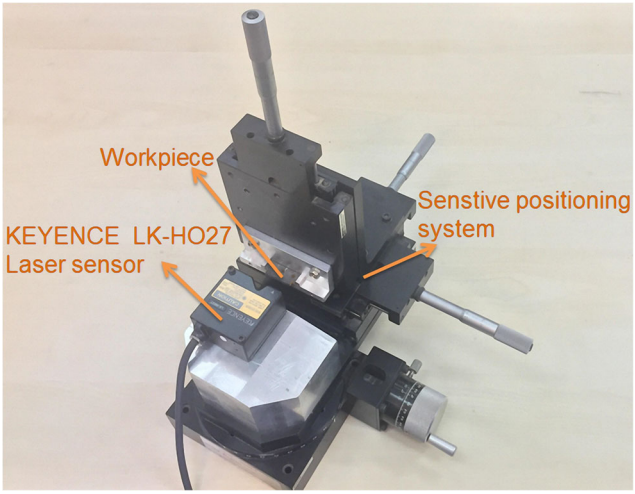

Fig. 11 Measurement setup

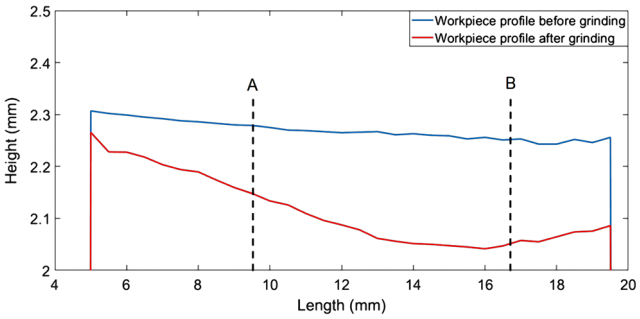

Fig. 12 Surface profile of the workpiece before grinding and after grinding operation without any force control

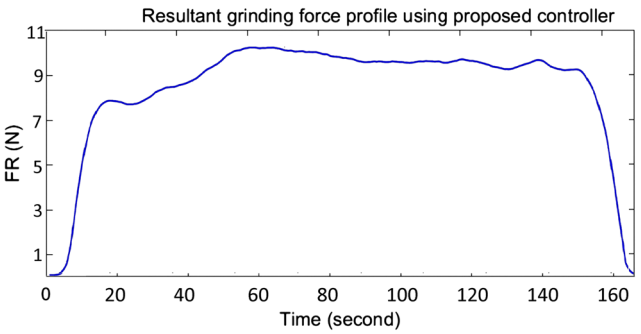

Fig. 14 Grinding resultant force profile using the proposed force control approach

setup resultant force is controlled by the fuzzy controller in order to track the reference force generated by the grinding force model. The input of the controller is the error between the reference force profile and resultant grinding force feedback measured by the sensor. During tool and workpiece interaction, to prevent any impulsive behaviors followed by unwanted overshoots and force fluctuations and probable tool and workpiece defects, both cutting depth and its rate of change should be controlled simultaneously. So, the outputs of the fuzzy controller are the necessary change in depth of cut (Δa_p) and its rate of change ($\Delta \dot{a_p}$). The mentioned fuzzy controller outputs are input to the piezo actuator. The architecture of the proposed admittance control structure is shown in Fig. 6.

In this study, nine Gaussian membership functions were designed for error, (Δa_p) and ($\Delta \dot{a_p}$) as shown in Figs. 7, 8, and 9 respectively.

The rule bases of the fuzzy controller are given in Table 2. The results and advantages of the proposed control strategy are presented in the next section.

7 Results and discussion

The general form of the proposed resultant grinding force control strategy is shown in the previous section. An example of the grinding resultant force profile without using a force controller and without implementing the TDC algorithm is shown in Fig. 10. A flat-shaped workpiece was used for this experiment.

As the normal, tangential, and resultant grinding forces increase almost linearly, this experiment belongs to the second grinding regime. Such a force increase is due to the tool deflection and low stiffness of the robotic grinding setup. The profile of the workpiece surface is measured by a Keyence-LK-HO27 laser distance sensor, shown in Fig. 11.

Due to the applied resultant force (Fig. 10), the profile produced on the surface is shown in Fig. 12 together with the original surface profile of the workpiece.

As shown in Fig. 12, the grinded surface profile shows the expected depth of cut increase along with the resultant force rise. It shows that the material removal rate is changing along the workpiece. Therefore, it is not possible to obtain desired cutting depth (SDOC) and desired constant material removal rate during the surface grinding operation which cause geometrical errors. The increase in the resultant force is due to tool deflection. Such a deflection adds an extra component to the grinding force continuously, and this component can be considered as a spring force.

Without implementing the TDC algorithm, a significant error occurs in the cross section of the workpiece. As shown in Fig. 13, an inclined cross section is obtained because of

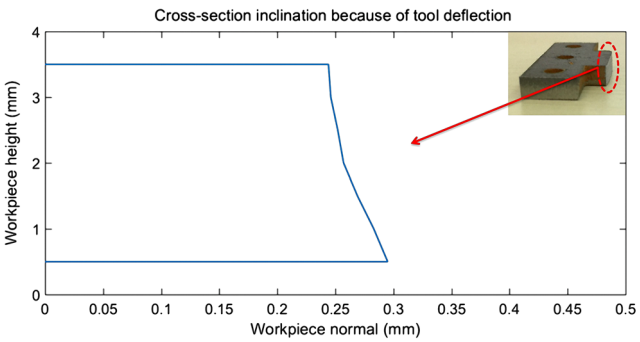

Fig. 13 Inclined cross section because of tool deflection

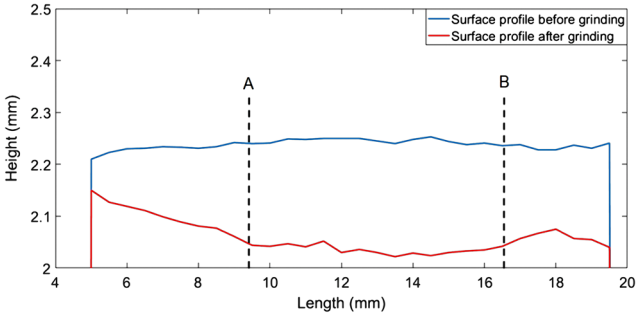

Fig. 15 Surface profile of the workpiece before grinding and after grinding operation using the proposed force control approach

the tool deflection. Such an inclination makes it difficult to control SDOC.

Applying the proposed control approach on the robotic grinding operation and trying to maintain a constant grinding resultant force led to the force graph shown in Fig. 14. In this graph, the force controller tries to maintain a resultant force of 9 N based on the grinding model output. In this experiment spindle speed is 30000 rpm, SDOC is 230 μm, feed rate is 0.1 mm/s, and percent load is 36%. The percent load value is selected based on maximum value of percent load in penetration test that is explained in Ref. [11].

In this research, in order to express the effect of the resultant grinding force on the workpiece profile, the force change is shown from tool and workpiece contact instant until tool exit, in parallel with the resulting workpiece profile. The measured surface profile of the workpiece after the grinding operation with resultant force control is shown in Fig. 15 together with the original workpiece surface profile before grinding operation. As shown in Fig. 15, by entering the tool to the workpiece, the cutting depth is increased. When the grinding force reaches to the reference resultant grinding force value, the controller keeps the resultant grinding force at the range of reference grinding force value. In this condition (point A to point B on the workpiece), the cutting depth remains almost constant until the tool begins to exit from workpiece. In both Figs. 12 and 15, there are increases in the last parts of the workpieces′ machined surfaces which means decrease in material removal rate. This increase starts when the tool begins to exit the workpiece. Consequently, the cutting force and the cutting depth decrease and this changes cause ascending in the workpiece profile graph. In this experiment, when the tool is completely in contact with the workpiece and without considering effect of tool entrance and tool exit (point A to point B on the workpiece), the average cutting depth is equal to 209 μm where the SDOC is equal to the 230 μm. Using the controller, the average error between actual and target cutting depth is equal to 21 μm. The maximum variation on the workpiece profile in this condition is equal to 30 μm. It means that using the resultant force control method, the cutting depth and surface quality remain constant with acceptable accuracy. Without using the proposed controller, the cutting force and consequently cutting depth increase until the tool starts to exit from the workpiece. The maximum variation on the workpiece profile in this condition is equal to 106 μm and the average cutting depth is equal to 185.5 μm. It means that without using any controller, the cutting depth and surface quality variate along the workpiece where the average error between actual and target cutting depth is equal to 44.5 μm. The target grinding accuracy in this study is 30 μm for the range of $200 - 250 \mu m$ cutting depth in one-cut machining. The achieved average accuracy was 21 μm. Note that the tool entrance and exit parts are not considered. It is important to note that without implementing TDC, due to the inclination of workpiece cross section, the above values are not meaningful for cutting depth values and operation accuracy.

The effect of TDC is shown in Fig. 16. Implementing the tool deflection compensation algorithm, a vertical cross section is obtained.

The motions of the hexapod in the x, y, and z directions while implementing the deflection compensation algorithm are shown in Fig. 17. Also, the hexapod rotations around the x, y, and z axes during operation are shown in Fig. 18. The motion in the y-direction decreases linearly because the feeding during operation is in the y-direction. The other motions and orientations are due to the outputs of the compensation algorithm.

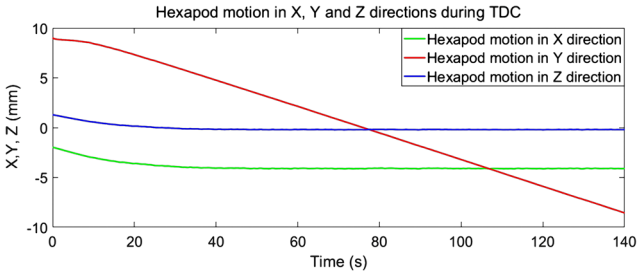

Fig. 17 Hexapod motion in the x, y, and z directions during the robotic grinding experiment

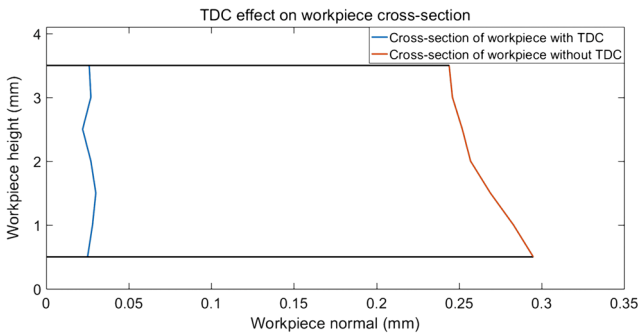

Fig. 16 Effect of the TDC algorithm on the workpiece cross section

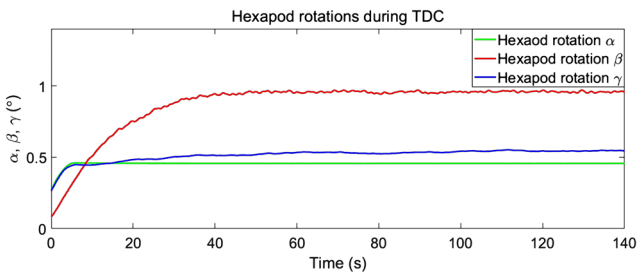

Fig. 18 Hexapod rotation around the x, y, and z axes during the robotic grinding experiment

One of the challenges of using fuzzy controllers is their stability check difficulty in different conditions. If a constant improper reference input is used, it is possible to encounter instabilities. However, the fuzzy approach is useful for controlling cutting depth and its rate of change simultaneously, but tuning this type of controller without using a model is problematic. The first advantage of the proposed control architecture is that due to its model-supervised nature, the reference force profile that should be tracked by the physical setup is realistic. This means that an improper reference force is guaranteed not to be given to the physical setup. Consequently, the unwanted grinding force overshoots and fluctuations followed by probable instabilities and tool or workpiece defects are prevented. Furthermore, application of the grinding model and the model-supervised controller facilitates the pre-simulation of the operation and tuning of the controller based on the desired controller characteristics.

8 Conclusions

In this study, a novel approach is proposed for parallel hexapod-robotic light abrasive grinding with constant resultant grinding force and real-time TDC. For this purpose, a model-supervised fuzzy admittance controller is proposed for the robotic grinding operation with constant resultant force. The robotic grinding behavior is different from grinding behavior with common CNC-type stiff machines. Due to tool deflection and the lower stiffness of the robotic grinding setup, three different regimes can be observed for the grinding force profile. A force prediction model is used in this study that is designed for robotic grinding operations. In grinding operation, the tool deflection is the main disadvantage which causes geometrical error (inclined profile) in the cross section of the workpiece. In this research, a method for calculation of tool deflection in tangential and normal directions is utilized, combined with a kinematic solution for real-time compensation of the tool deflection. Application of this approach leads to obtain disinclined cross section.

Investigating the results of experiments, the following inferences are concluded.

- Resultant force control is an effective method for preventing geometrical errors in robotic grinding operation.
- The resultant grinding force can be adjusted in real time by controlling the depth of cut and its rate of change.
- The tuned realistic reference input produced by the force model, combined with the functionality of the fuzzy controller for nonlinear plants, provides a proper method for increasing the accuracy of robotic grinding operations.
- The proposed model-supervised fuzzy control structure decreases the instability probability of the fuzzy controller because of the realistic reference input profile produced by the grinding model.
- Computation of the tool deflection value as a function of grinding forces and compensation of it in real time during the robotic grinding operation is an effective way of preventing geometrical errors in workpiece cross-section.

Funding information We would like to thank the Scientific and Technological Research Council of Turkey for their financial support of this research under Grant TUBITAK -114E274.

References

1. Budak E (2000) Improving productivity and part quality in milling of titanium based impellers by chatter suppression and force control. Annals of the CIRP 49(1):31–36
2. Budak E, Tunc LT, Alan S, Özgüven N (2012) Prediction of workpiece dynamics and its effects on chatter stability in milling. CIRP Ann Manuf Technol 61:339–342. https://doi.org/10.1016/j.cirp.2012.03.144
3. Campa FJ, de Lacalle LLN, Lamikiz A, Bilbao E, Calleja A, Penafiel J (2009) Tool deflection on peripheral milling. The Annals of Dunarea de Jos University of Galati Fascicle V, Technologies in Machine Building pp 169–174
4. Denkena B, Möhring HC, Will JC (2007) Tool deflection compensation with an adaptronic milling spindle. In: Conference on smart machining systems
5. Domroes F, Krewet C, Kuhlenkoetter B (2013) Application and analysis of force control strategies to deburring and grinding. Modern Mechanical Engineering 3(June):11–18. https://doi.org/10.4236/mme.2013.32A002
6. Fang F, Wu H, Liu Y (2005) Modelling and experimental investigation on nanometric cutting of monocrystalline silicon. Int J Mach Tools Manuf 45(15):1681–1686
7. Habibi M, Arezoo B, Vahebi Nojedeh M (2011) Tool deflection and geometrical error compensation by tool path modification. Int J Mach Tools Manuf 51(6):439–449. https://doi.org/10.1016/j.ijmachtools.2011.01.009
8. Jung S, Hsia TC, Bonitz RG (2004) Force tracking impedance control of robot manipulators under unknown environment. IEEE Trans Control Syst Technol 12(3):474–483
9. Kline WA, Devor RE, Shareef IA (1982) The prediction of surface accuracy in end milling. In: Trans, of ASME, vol 104, pp 272–278. https://doi.org/10.1115/1.3185830
10. López de Lacalle LN, Lamikiz A, Sanchez J, Salgado M (2007) Toolpath selection based on the minimum deflection cutting forces in the programming of complex surfaces milling. Int J Mach Tools Manuf 47(2):388–400
11. Latifinavid M, Konukseven EI (2017) Hybrid model based on energy and experimental methods for parallel hexapod-robotic light abrasive grinding operations. Int J Adv Manuf Technol 93:3873. https://doi.org/10.1007/s00170-017-0798-8
12. Law KMY, Geddam A, Ostafiev VA (1999) A process-design approach to error compensation in the end milling of pockets. J Mater Process Technol 89–90:238–244. https://doi.org/10.1016/S0924-0136(99)00031-X
13. Li D, Xu M, Wei C (2012) A dynamic threshold-based fuzzy adaptive control algorithm for hard sphere grinding. Int J Adv Manuf Technol 60:923–932. https://doi.org/10.1007/s00170-011-3661-3

14. Liu C, Chen A, Wang YT, Chen CC (2004) Modelling and simulation of an automatic grinding system using a hand grinder. Int J Adv Manuf Technol 23:874–881. https://doi.org/10.1007/s00170-003-1736-5
15. Liu CC, Chen A, Chen CCC, Wang YYT (2005) Grinding force control in an automatic surface finishing system. J Mater Process Technol 170(1-2):367–373. https://doi.org/10.1016/j.jmatprotec.2005.06.002
16. Lopez de Lacalle LN, Lamikiz A, Sanchez JA, Salgado MA (2004) Effects of tool deflection in the high-speed milling of inclined surfaces. Int J Adv Manuf Technol 24:621–631. https://doi.org/10.1007/s00170-003-1723-x
17. de Lacalle LLN, Lamikiz A, Sánchez JA, Bustos IFD (2005) Simultaneous measurement of forces and machine tool position for diagnostic of machining tests. IEEE Trans Instrum Meas 54(6):2329–2335
18. de Lacalle LLN, Lamikiz A, Sánchez JA, Salgado MA (2007) Toolpath selection based on the minimum deflection cutting forces in the programming of complex surfaces milling. Int J Mach Tools Manuf 47(2):388–400. https://doi.org/10.1016/j.ijmachtools.2006.03.010
19. Luo J (ed.) (2012) Soft computing in information communication technology (Vol. 2). Springer Science & Business Media
20. Mendes N, Neto P, Pires JN, Loureiro A (2013) An optimal fuzzy-PI force / motion controller to increase industrial robot autonomy. Int J Adv Manuf Technol 68:435–441. https://doi.org/10.1007/s00170-013-4741-3
21. Nieslony P, Krolczyk G, Wojciechowski S, Chudy R, Zak K, Maruda R (2018) Surface quality and topographic inspection of variable compliance part after precise turning. Appl Surf Sci 434:91–101
22. Özgören MK (2002) Topological analysis of 6-joint serial manipulators and their inverse kinematic solutions. Mech Mach Theory 37(5):511–547. https://doi.org/10.1016/S0094-114X(02)00005-8
23. Ozgoren MK (2007) Kinematic analysis of spatial mechanical systems using exponential rotation matrices. J Mech Des 129(11):1144. https://doi.org/10.1115/1.2771233
24. Özgören MK (2013) Optimal inverse kinematic solutions for redundant manipulators by using analytical methods to minimize position and velocity measures. J Mech Robot 5(3):031,009. https://doi.org/10.1115/1.4024294
25. Pagilla P, Yu B (2001) Adaptive control of robotic surface finishing processes. In: Proceedings of the 2001 american control conference. (cat. no.01CH37148), vol 1, pp 630–635. https://doi.org/10.1109/ACC.2001.945617
26. Rao VS, Rao PVM (2006) Effect of workpiece curvature on cutting forces and surface error in peripheral milling. Proc Inst Mech Eng B J Eng Manuf 220(9):1399–1407
27. Rao VS, Rao PVM (2006) Tool deflection compensation in peripheral milling of curved geometries. Int J Mach Tools Manuf 46(15):2036–2043. https://doi.org/10.1016/j.ijmachtools.2006.01.004
28. Ryu SH, Lee HS, Chu CN (2003) The form error prediction in side wall machining considering tool deflection. Int J Mach Tools Manuf 43:1405–1411. https://doi.org/10.1016/S0890-6955(03)00183-4
29. Soori M, Arezoo B, Habibi M (2014) Virtual machining considering dimensional, geometrical and tool deflection errors in three-axis CNC milling machines. J Manuf Syst 33(4):498–507. https://doi.org/10.1016/j.jmsy.2014.04.007
30. Suh SH, Cho JH, Hascoet JY (1996) Incorporation of tool deflection in tool path computation: simulation and analysis. J Manuf Syst 15(3):190–199
31. Tao Y, Zheng J, Lin Y, Wang T, Xiong H, He G, Xu D (2015) Fuzzy PID control method of deburring industrial robots. J Intell Fuzzy Syst 29(6):2447–2455. https://doi.org/10.3233/IFS-151945
32. Thomessen T, Lien TK, Sannñs PK (2001) Robot control system for grinding of large hydro power turbines. Industrial Robot: An International Journal 28(4):328–334
33. Wang S, To S, Cheung C (2013) An investigation into material-induced surface roughness in ultra-precision milling. Int J Adv Manuf Technol 68(1-4):607–616
34. Wojciechowski S, Maruda R, Barrans S, Nieslony P, Krolczyk G (2017) Optimisation of machining parameters during ball end milling of hardened steel with various surface inclinations. Measurement 111:18–28
35. Wojciechowski S, Maruda RW, Krolczyk GM, Niesłony P (2018) Application of signal to noise ratio and grey relational analysis to minimize forces and vibrations during precise ball end milling. Precis Eng 51:582–596
36. Yang MY, Choi JG (1998) A tool deflection compensation system for end milling accuracy improvement. J Manuf Sci Eng 120(2):222–229
37. Yang Z, Gao Y, Zhang D, Huang T (2003) A self-tuning based fuzzy-PID approach for grinding process control. Key Engineering Materials Trans Tech Publications 238–239:375–382
38. Zeng G (1997) An overview of robot force control. Robotica 15(5):473–482